EDDY CURRENT TOMOGRAPHY OF DEPOSITS IN STEAM GENERATOR

Zixian Jiang[1], *Mabrouka El Guedri*[2], *Houssem Haddar*[1], *and Armin Lechleiter*[1]

1. INRIA Saclay and CMAP, Ecole Polytechnique
route de Saclay, 91128, Palaiseau, France
phone: + 33 1 6933 4584, fax: + 33 1 6933 4646,
email: zixian.jiang@polytechnique.edu,
haddar@cmap.polytechnique.fr,
alechle@cmap.polytechnique.fr

2. STEP, EDF R&D
6 quai Waltier, 78400, Chatou, France
phone: + 33 1 3087 8501
email: mabrouka.el-guedri@edf.fr

ABSTRACT

Eddy current testing (ECT) using coils is widely practised in in-service inspection of steam generators in nuclear power plants of pressurized water reactor type. In this paper, we consider the shape estimate problem of magnetic deposits given some ECT signals. The non-linearity and the ill-posedness of this inverse problem make it quite challenging. We focus on the axisymmetric case and build a PDE-based direct model with Dirichlet-to-Neumann boundary operators to describe the relationship between observed data and the inspected component. With this direct model, we propose an inverse algorithm of gradient descent shape optimization type involving a regularization technique by boundary differential operators. First numerical experiments are quite encouraging.

1. INTRODUCTION: INDUSTRY BACKGROUND

Steam Generators (SGs) are critical components in nuclear power plants. Through SG tubes, heat produced in a nuclear reactor core and transferred by the primary loop in SG tubes boils coolant water in the secondary loop on the shell side into steam, which is then delivered to steam turbines. Magnetic deposits usually observed on the shell side of SG tubes could, however, affect the power production and even the structure security. So eddy current inspection is applied to detect presence, shape and/or physical nature of deposit.

In ECT, a probe consists of two coils of wire, each connected to a current generator producing an alternating current and a voltmeter measuring the the voltage change across the coil. Once the probe is introduced in the SG tube, the generator coil excited by the current creates a primary electromagnetic field which in turn induces a current flow in the electrically conductive material nearby, such as the tube. The presence of magnetic deposit will distort the flow of eddy currents. They induce a current change in the receiver coil which is measured in terms of impedance, called ECT signals.

We aim to estimate the deposit shape given ECT signals by supposing that the physical nature of deposit is known.

2. PROBLEM STATEMENT

In this section, we state the deposit shape reconstruction given ECT signals as an inverse problem based on a direct problem with preliminary sets.

2.1 Notations

- $\mathrm{i} = \sqrt{-1}$: the imaginary unit;
- ω, I, J: frequency, intensity and distribution of the primary alternating current;
- Ω_i, μ_i, σ_i: domain, permeability and conductivity; $i = 0$ for vacuum, $i = T$ for tube, $i = D$ for deposit; $\mu_0 = \mu_T$;
- μ^0, σ^0: permeability and conductivity distributions in deposit free situation, and μ, σ those in general case;
- u^0, u: azimuthal components of the electric fields, respectively in the deposit free case and in the general case with contingent deposit, and u_k^0 or u_k for those fields induced by the coil k.

2.2 Direct problem

We suppose the rotational symmetry with respect to the axis of the SG tube. Thus the 3-D problem in the cylindrical coordinate system (r,θ,z) turns to a 2-D case in the semi-plane, noted $\mathbb{R}^2_+ = \{(r,z) : r \in \mathbb{R}_+, z \in \mathbb{R}\}$ (see Figure 1).

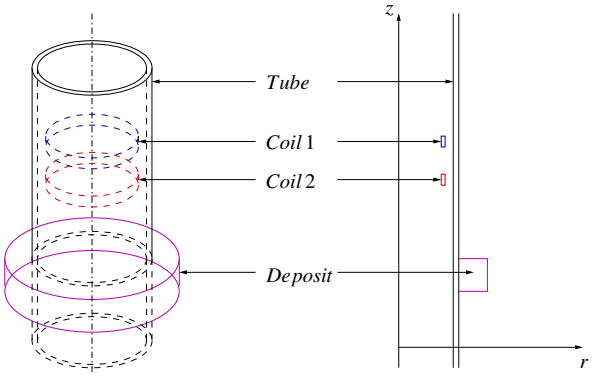

Figure 1: 3-D and 2-D geometrical representations

By solving the direct problem proposed in Section 3, we obtain the non-zero azimuthal components of electric fields u (or u^0) for configurations with (or without) magnetic deposit.

2.3 ECT signals

By adapting equation $(10a)$ in [2] to our case, the impedance measured for the coil k in the electromagnetic field induced by the coil l writes

$$\triangle Z_{kl} = \triangle Z_l(u_k) = -\frac{2\pi}{I^2}\int_{\Omega_D}\left(\frac{1}{\mathrm{i}\omega}\frac{\mu-\mu^0}{\mu\mu^0}\frac{1}{r^2}\nabla(ru_k)\cdot\nabla(ru_l^0) + (\sigma-\sigma^0)u_k u_l^0\right) r\,\mathrm{d}r\,\mathrm{d}z. \quad (1)$$

Further measurements can be obtained with different combinations of $\triangle Z_{kl}$, $k,l = 1,2$. In industry application, as mentioned in [4], ECT signals are recorded in two modes with a certain frequency ($\omega = 100\,kHz$),

$$\begin{cases} Z_{F3} = \dfrac{\mathrm{i}}{2}(\triangle Z_{11} - \triangle Z_{22}) & \text{differential mode,} \\ Z_{FA} = \dfrac{\mathrm{i}}{2}(\triangle Z_{11} + \triangle Z_{12}) & \text{absolute mode.} \end{cases} \tag{2}$$

For exemple, Figure 2 gives the ECT signals deformed by a rectangular deposit described in Section 5. We denote by $Z(\Omega_D;\zeta)$ either $Z_{F3}(\Omega_D;\zeta)$ or $Z_{FA}(\Omega_D;\zeta)$ (see (2)) the ECT signals measured at the probe position $\zeta \in \mathbb{R}$.

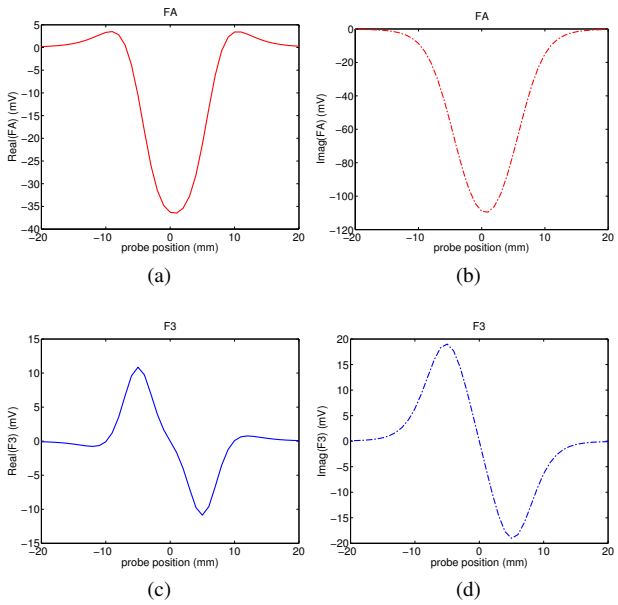

Figure 2: ECT signals distorted by a rectangular deposit. (a) FA real part; (b) FA imaginary part; (c) F3 real part; (d) F3 imaginary part.

Supposing that the deposit material is homogeneous with known permeability μ_D and conductivity σ_D. From the ECT signal expressions (1) and (2), the shape of the deposit Ω_D determines u_k and thus the impedance measurements.

2.4 Inverse problem

In an eddy current inspection, we make a scan by moving the probe along the axis of the SG tube from position $z_{\min}$ to $z_{\max}$. The inverse problem aims to approximate the unknown deposit shape Ω_D^* given the ECT signals $Z(\Omega_D^*;\zeta)$ for $z_{\min} \leq \zeta \leq z_{\max}$. Rather than the contrast source inverse method that the preceding works used (see [5] and its references), we take the shape optimization approach to minimize the cost functional

$$J(\Omega_D) = \int_{z_{\min}}^{z_{\max}} |Z(\Omega_D;\zeta) - Z(\Omega_D^*;\zeta)|^2 \,\mathrm{d}\zeta, \tag{3}$$

with the gradient descent method, which requires to calculate the shape derivative, presented in Section 4.1. Compared to the contrast source inversion, the advantage of this approach is that it considers the boundary of deposit and gives a precise continuous edge as result.

Due to the ill-posedness of the inverse problem (see for example [5]), the shape increment given by a first approach (see Section 4.2 may develop sharp oscillations during the minimization process when the number of discretization points of $\partial\Omega_D^0$ is high. These oscillations might cause divergence of the algorithm (see Section 5.2 for a numerical example). This is why a regularization procedure needs to be incorporated (readers may refer to [3] for a general introduction to the regularization of inverse problems). With the boundary regularization method showed in Section 4.3, the shape optimization scheme becomes stable.

3. EDDY CURRENT MODEL

In this section, we solve the direct problem based on the eddy current model. From Maxwell's equations and the eddy current hypothesis on small electric permittivity compared to conductivity, that is $\varepsilon \ll \sigma/\omega$, we get the 2-D second order eddy current equation for azimuthal component of electric field u in a cylindric coordinate system:

$$\mathrm{div}\left(\frac{1}{\mu r}\nabla(ru)\right) + \mathrm{i}\omega\sigma u = -\mathrm{i}\omega J, \quad \text{in } \mathbb{R}^2_+. \tag{4}$$

The electric field vanishes in other directions in a rotational symmetric case. We have also a condition at infinity and a boundary condition at $r = 0$ due to symmetry:

$$u(r,z) \to 0 \quad (r \to \infty), \tag{5}$$
$$u|_{r=0} = 0. \tag{6}$$

The unbounded domain $\mathbb{R}^2_+$ in (4) is, for the sake of numerical resolution, reduced to B_{r_0,z_0} with $r_0 > 0$ and $z_0 > 0$. Therefore, we introduce three new boundaries:

$$\Gamma_{r_0} = \{(r,z) : r = r_0, -z_0 \leq z \leq z_0\}, \quad \text{and}$$
$$\Gamma_{\pm} = \{(r,z) : 0 \leq r \leq r_0, z = \pm z_0\}.$$

To simplify the model, we replace the condition at infinity in r direction (5) by a homogenous Dirichlet boundary condition on Γ_{r_0} for r_0 large enough: $u|_{\Gamma_{r_0}} = 0$. Similar homogeneous Dirichlet boundary conditions can also be posed on $\Gamma_{\pm}$ for z_0 large enough. But for the sake of numerical precision as well as efficiency, we will introduce **Dirichlet-to-Neumann** (D-t-N) operators on $\Gamma_{\pm}$ in a formal way.

For z_0 such that the current density $J = 0$ for all $|z| \geq z_0$, we have

$$\mathrm{div}\,(\frac{1}{r}\nabla(ru)) + \mathrm{i}\omega\sigma\mu u = 0 \tag{7}$$

A separation of the variables $u(r,z) = \rho(r)\zeta(z)$ gives an eigenvalue problem

$$\frac{\zeta''(z)}{\zeta(z)} = -\frac{\rho''(r)}{\rho(r)} - \frac{\rho'(r)}{r\rho(r)} + \frac{1}{r^2} - \mathrm{i}\omega\mu\sigma = \lambda. \tag{8}$$

We note λ_n the eigenvalues for the problem of ρ and $\rho_n(r)$ the corresponding eigenvectors. Thus

$$u(r,z) = \sum_{n\in\mathbb{N}} u_n\rho_n(r)\exp(-\sqrt{\lambda_n}(z-z_0)), \quad z \geq z_0,$$

and similar results for $z \leq z_0$.

For any $\varphi(r)$ defined on Γ_+ with decomposition $\varphi(r) = \sum_{n\in\mathbb{N}} \varphi_n \rho_n(r)$, we define the D-t-N operator

$$\mathscr{T}_+ \varphi = \sum_{n\in\mathbb{N}} (-\sqrt{\lambda_n})\varphi_n \rho_n(r).$$

In the same way, we can define a D-t-N operator $\mathscr{T}_-$ on Γ_-. So for u the solution to problem (4) – (6), we have

$$\left.\frac{\partial u}{\partial z}\right|_{\Gamma_\pm} = \mathscr{T}_\pm(u|_{\Gamma_\pm}).$$

We define the following functional spaces:

$$H_r^1(B_{r_0,z_0}) := \left\{ v : v\sqrt{r},\ \frac{v}{\sqrt{r}},\ \frac{\partial v}{\partial r}\sqrt{r},\ \frac{\partial v}{\partial z}\sqrt{r} \in L^2(B_{r_0,z_0}) \right\},$$
$$H := \left\{ v \in H_r^1(B_{r_0,z_0}) : v|_{r=0} = 0,\ v|_{\Gamma_R} = 0 \right\}.$$

So the equivalent variational formulation of the problem (4)-(6) is:

$$a(u,v) - \int_{\Gamma_+} \frac{1}{\mu}\mathscr{T}_+(u|_{\Gamma_+})\bar{v}r\,\mathrm{d}s - \int_{\Gamma_-} \frac{1}{\mu}\mathscr{T}_-(u|_{\Gamma_-})\bar{v}r\,\mathrm{d}s$$
$$= \int_{B_{r_0,z_0}} \mathrm{i}\omega J\bar{v}r\,\mathrm{d}r\,\mathrm{d}z, \quad \forall v \in H. \tag{9}$$

where

$$a(u,v) = \int_{B_R} \left(\frac{1}{\mu r^2}\nabla(ru)\cdot\nabla(r\bar{v}) - \mathrm{i}\omega\sigma u\bar{v} \right) r\,\mathrm{d}r\,\mathrm{d}z. \tag{10}$$

A slight modification of Poincaré inequality shows that the sesquilinear form $a(\cdot,\cdot)$ defined on $H\times H$ by (10) is elliptic. Therefore the Lax-Milgram theorem yields the existence and uniqueness of solution to the problem (9).

The variational problem (9) is numerically solved with the help of the finite element package `FreeFem++` (see `www.freefem.org`).

4. INVERSE ALGORITHM

In this section, we give an inverse algorithm for the deposit shape reconstruction. We recall the cost functional (3) to be minimized

$$J(\Omega_D) = \int_{z_{\min}}^{z_{\max}} |Z(\Omega_D;\zeta) - Z(\Omega_D^*;\zeta)|^2\,\mathrm{d}\zeta.$$

The gradient descent shape optimization involves the notion of shape derivative (see Section 4.1). Then the minimizing shape increment is regularized by introducing a boundary differential operator (see Section 4.3) so that the optimization process is stable and converges.

4.1 Shape derivative of the cost functional

Shape derivative methods are detailed in [1]. To simplify the introduction, we only discuss the case that the deposit is pure conductor, i.e. $\mu_D = \mu_0$. If the original deposit domain Ω_D^0 is deformed by a shape perturbation $\boldsymbol{\theta}$: $\Omega_D = (\mathrm{Id}+\boldsymbol{\theta})\Omega_D^0$, then the shape derivative of $J(\Omega_D)$, noted as $J'(\Omega_D^0)(\boldsymbol{\theta})$, is defined by

$$J(\Omega_D) = J(\Omega_D^0) + J'(\Omega_D^0)(\boldsymbol{\theta}) + o(\boldsymbol{\theta}), \quad \lim_{\boldsymbol{\theta}\to 0}\frac{\|o(\boldsymbol{\theta})\|}{\|\boldsymbol{\theta}\|} = 0.$$

Analogously are defined shape derivatives Z' and $\triangle Z'_{kl}$ of Z and $\triangle Z_{kl}$ (see (1)). Then we have

$$J'(\Omega_D^0)(\boldsymbol{\theta}) = \int_{z_{\min}}^{z_{\max}} 2\Re\left\{ Z'(\Omega_D^0;\zeta)(\boldsymbol{\theta})\overline{\left(Z(\Omega_D^0;\zeta) - Z(\Omega_D^*;\zeta)\right)} \right\}\mathrm{d}\zeta.$$

From (2), we shall calculate $\triangle Z'_{kl}(\Omega_D)(\boldsymbol{\theta})$ indeed. Since μ is constant, from (1), its shape derivative is

$$\triangle Z'_{kl}(\Omega_D^0)(\boldsymbol{\theta}) = -\frac{2\pi}{I^2}\left(\int_{\Omega_D^0} (\sigma-\sigma^0)u'_k u_l^0 r\,\mathrm{d}r\,\mathrm{d}z + \int_{\partial\Omega_D^0} (\boldsymbol{\theta}\cdot\boldsymbol{n})[\sigma]u_k u_l^0 r\,\mathrm{d}s \right), \tag{11}$$

where $u'_k = u'$ is the Eulerian shape derivative of u according to the perturbation $\boldsymbol{\theta}$:

$$u(\Omega_D;r,z) = u(\Omega_D^0;r,z) + u'(\boldsymbol{\theta};\Omega_D^0;r,z) + o(\boldsymbol{\theta}).$$

Then u' is the unique solution to the variational formulation problem:

$$a(u',v) - \int_{\Gamma_+} \frac{1}{\mu}\mathscr{T}_+(u'|_{\Gamma_+})\bar{v}r\,\mathrm{d}s - \int_{\Gamma_-} \frac{1}{\mu}\mathscr{T}_-(u'|_{\Gamma_-})\bar{v}r\,\mathrm{d}s$$
$$= \int_{\partial\Omega_D^0} (\boldsymbol{\theta}\cdot\boldsymbol{n})\mathrm{i}\omega[\sigma]u\bar{v}r\,\mathrm{d}s, \quad \forall v \in H. \tag{12}$$

4.2 Expression of the derivative using the adjoint state

To u_l^0 solution to a deposit free eddy current problem, we associate an adjoint state p_l solution to the problem

$$\begin{cases} \mathrm{div}\left(\frac{1}{\mu r}\nabla(rp_l)\right) + \mathrm{i}\omega\sigma p_l = \mathrm{i}\omega(\sigma-\sigma^0)u_l^0 & \text{in } B_{r_0,z_0} \\ p_l = 0 & \text{on } \partial B_{r_0,z_0}. \end{cases}$$

Its equivalent variational formulation is,

$$a(p_l,v) = -\int_{B_{r_0,z_0}} \mathrm{i}\omega(\sigma-\sigma^0)u_l^0\bar{v}r\,\mathrm{d}r\,\mathrm{d}z, \quad \forall v \in \widetilde{H}, \tag{13}$$

where $\widetilde{H} := \{v \in H : v|_{\Gamma_\pm} = 0\}$.

From (11), (12) and (13), and some calculations, we get

$$\triangle Z'_{kl}(\Omega_D^0)(\boldsymbol{\theta}) = \int_{\partial\Omega_D^0} (\boldsymbol{\theta}\cdot\boldsymbol{n})[\sigma]u_k(p_l - u_l^0)r\,\mathrm{d}s.$$

Thus, for impedance in the differential mode Z_{F3},

$$Z'_{F3}(\Omega_D^0)(\boldsymbol{\theta}) = \frac{\mathrm{i}\pi}{I^2}\int_{\partial\Omega_D^0} (\boldsymbol{\theta}\cdot\boldsymbol{n})\,[\sigma]\left(u_1(p_1-u_1^0) - u_2(p_2-u_2^0)\right)r\,\mathrm{d}s,$$

and for that in the absolute mode Z_{FA},

$$Z'_{FA}(\Omega_D^0)(\boldsymbol{\theta}) = \frac{\mathrm{i}\pi}{I^2}\int_{\partial\Omega_D^0} (\boldsymbol{\theta}\cdot\boldsymbol{n})\,[\sigma]\left(u_1(p_1-u_1^0) + u_1(p_2-u_2^0)\right)r\,\mathrm{d}s.$$

Let us define:

$$\begin{cases} g_{F3}(r,z) = \displaystyle\int_{z_{\min}}^{z_{\max}} \Re\Big\{ \big(u_1(p_1-u_1^0) - u_2(p_2-u_2^0)\big)(r,z;\zeta) \\ \qquad\qquad \overline{\big(Z(\Omega_D^0;\zeta) - Z(\Omega_D^*;\zeta)\big)}(-\mathrm{i}) \Big\}\,\mathrm{d}\zeta, \\ g_{FA}(r,z) = \displaystyle\int_{z_{\min}}^{z_{\max}} \Re\Big\{ \big(u_1(p_1-u_1^0) + u_1(p_2-u_2^0)\big)(r,z;\zeta) \\ \qquad\qquad \overline{\big(Z(\Omega_D^0;\zeta) - Z(\Omega_D^*;\zeta)\big)}(-\mathrm{i}) \Big\}\,\mathrm{d}\zeta. \end{cases} \tag{14}$$

Then the shape derivative of the cost functional becomes

$$J'(\Omega_D^0)(\boldsymbol{\theta}) = -\frac{2\pi}{I^2}\int_{\partial\Omega_D^0} (\boldsymbol{\theta}\cdot\boldsymbol{n})\,[\sigma]\,g r\,\mathrm{d}s, \tag{15}$$

where the function g is either g_{F3} or g_{FA} according to the chosen measuring mode.

To ensure that the cost functional decreases, we can take a perturbation of the geometry Ω_D^0 such that:

$$\boldsymbol{\theta}|_{\partial\Omega_D^0} = [\sigma]\,g|_{\partial\Omega_D^0}\,r\boldsymbol{n}. \tag{16}$$

The perturbation can be calculated in the whole domain by solving the interior problem

$$\begin{cases} -\triangle\boldsymbol{\theta} = 0 & \text{in } \Omega_D^0, \\ \boldsymbol{\theta} = [\sigma]\,g|_{\partial\Omega_D^0}\,r\boldsymbol{n} & \text{on } \partial\Omega_D^0, \end{cases}$$

and the exterior problem

$$\begin{cases} -\triangle\boldsymbol{\theta} = 0 & \text{in } \mathscr{V}\setminus\Omega_D^0, \\ \boldsymbol{\theta} = 0 & \text{on } \partial\mathscr{V}, \\ \boldsymbol{\theta} = [\sigma]\,g|_{\partial\Omega_D^0}\,r\boldsymbol{n} & \text{on } \partial\Omega_D^0, \end{cases}$$

where $\boldsymbol{n}$ is always the outward normal unit of Ω_D^0 and $\mathscr{V}$ is a neighbourhood of Ω_D^0. The vector field $\boldsymbol{\theta}$ is extended by zero outside $\mathscr{V}$ to ensure that the shape perturbation would not change other geometrical configuration.

One easily verifies that

$$J'(\Omega_D^0)(\boldsymbol{\theta}) = -\frac{2\pi}{I^2}\int_{\partial\Omega_D^0} |\boldsymbol{\theta}|^2\,\mathrm{d}s \le 0.$$

4.3 Regularization

As mentioned in Section 2.4, a regularization is needed since the shape increment given by (16) may cause singularity on $\partial\Omega_D^0$. We propose to use the $H^1(\partial\Omega_D^0)$ boundary regularization by solving the following problem for $\boldsymbol{\lambda}\in H^1(\partial\Omega_D^0)^2$:

$$\boldsymbol{\lambda} - \alpha\triangle_{\partial\Omega_D^0}\boldsymbol{\lambda} = [\sigma]\,g|_{\partial\Omega_D^0}\,r\boldsymbol{n} \quad \text{on } \partial\Omega_D^0, \tag{17}$$

where $\triangle_{\partial\Omega_D^0}$ is the boundary Laplace-Beltrami operator and $\alpha>0$ is a regularization parameter. The equivalent variational formulation of (17) is,

$$\begin{aligned} &\int_{\partial\Omega_D^0}\Big(\boldsymbol{\lambda}\cdot\boldsymbol{\psi} + \alpha\nabla_{\partial\Omega_D^0}\boldsymbol{\lambda}\cdot\nabla_{\partial\Omega_D^0}\boldsymbol{\psi}\Big)\,\mathrm{d}s \\ &= \int_{\partial\Omega_D^0}[\sigma]\,g r\boldsymbol{n}\cdot\boldsymbol{\psi}\,\mathrm{d}s, \quad \forall\boldsymbol{\psi}\in H^1(\partial\Omega_D^0)^2. \end{aligned} \tag{18}$$

Compared to the right-side term in (16), we gain two regularity orders with $\boldsymbol{\lambda}$. We will take a shape perturbation $\boldsymbol{\theta}$ such that

$$\boldsymbol{\theta}|_{\partial\Omega_D^0} = \boldsymbol{\lambda}. \tag{19}$$

It is also a descent direction since we have, by taking $\boldsymbol{\psi} = \boldsymbol{\lambda} = \boldsymbol{\theta}|_{\partial\Omega_D^0}$ in (18),

$$J'(\Omega_D^0)(\boldsymbol{\theta}) = -\frac{2\pi}{I^2}\int_{\partial\Omega_D^0}\left(|\boldsymbol{\theta}|^2 + \alpha\left|\nabla_{\partial\Omega_D^0}\boldsymbol{\theta}\right|^2\right)\mathrm{d}s \le 0. \tag{20}$$

We can also extend $\boldsymbol{\theta}|_{\partial\Omega_D^0}$ to the whole domain as above.

4.4 Algorithm

The inversion procedure is done as follows:

- Initialization with a deposit domain Ω_D^0.
- Step k :
  1. Solve the direct problem (9) and the adjoint problem (4.2) with the actual deposit domain Ω_D^k.
  2. Calculate the cost functional with (3) and the according g function with (14).
  3. Get a descent direction $\boldsymbol{\theta}^k$ (see (19)) with a regularization procedure (17), calculate the shape derivative of the cost functional $J'(\Omega_D^k)(\boldsymbol{\theta}^k)$ with (20).
  4. Compare with the chosen optimization criteria. If they are not satisfied, go to step $k+1$ with a deposit domain
  $$\Omega_D^{k+1} = (\mathrm{Id}+\boldsymbol{\theta}^k)\Omega_D^k.$$

5. NUMERICAL TEST

We give some numerical test results in this section.

5.1 Application to a parametric problem

In the first place, we use a parametric case to test the shape optimization algorithm in Section 4.4. If we know *a priori* that the deposit domain is rectangular in the semi-plan $\mathbb{R}^2_+$ with fixed height (in the z direction), then it is parameterized by its length in the r direction. In the absolute mode (FA) of impedance measurement, we set:

- $\sigma_D = 1\times10^4\,S\cdot m^{-1}$, $\mu_D = \mu_0$;
- Fixed height is $10\,mm$;
- Target length is $5\,mm$; initialization with $1\,mm$ in length.

The exact shape and the initialization are shown in Figure 3a. After 92 iterative steps, we obtain the final shape shown in Figure 3b. Its length is $4.89\,mm$. A more general case is considered by only supposing the rectangular shape, but with unknown height as well as length. The exact shape and the initialization are shown in Figure 3c and the reconstruction after 24 steps is given in Figure 3d.

We remark that no regularization is needed in this case, since we have set strong hypothesis on the deposit shape (as rectangular).

5.2 Application to a general problem

Let us consider the general case now. In Figure 4a, the target deposit in green is always rectangular, but included in a neighbourhood $\mathscr{V}$, which is the support of the shape perturbation. We can find the boundary $\partial\mathscr{V}$ outside the deposit.

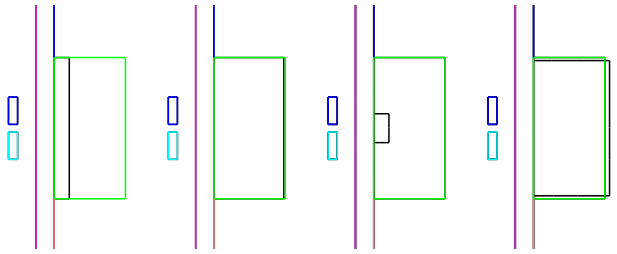

Figure 3: Reconstruction for parameterized problems with rectangular deposit target. (a)-(b) case with unknown length; (c)-(d) case with unknown height and length. In green: target shape. In black: (a), (c) initializations; (b), (d) reconstructions.

Since we do not know the domain shape *a priori*, we choose to initialize with a small semi-disc (in black).

An optimization process without regularization ends up, after 104 iterative steps, by the presence of sharp oscillations on the boundary, shown in Figure 4b. That shows the ill-posedness of the inverse problem and the instability of the shape optimization scheme for minimizing the cost functional.

With the boundary regularization method introduced in Section 4.3, the inverse algorithm gets stable and converges. We obtain the deposit shape shown in Figure 4c, after 60 iterative steps. The reconstructed shape represents a good approximation of the target in terms of volume. The inverse algorithm cannot recover the two angles of the rectangular since they are far from the probe, that the integration effect (see (1)) and the boundary regularization "smooths" their impact on ECT signals.

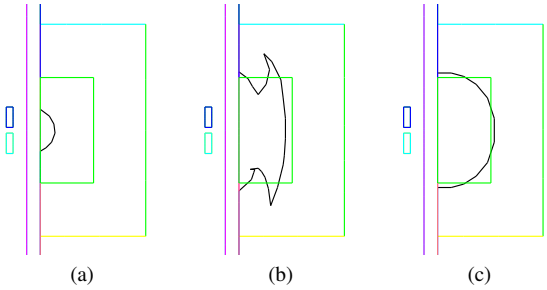

Figure 4: General problem with rectangular deposit target. In green: target shape. In black: (a) initialization; (b) reconstruction without regularization; (c) reconstruction with regularization.

We can consider other shape reconstructions as semi-disc (Figure 5) with the same inverse algorithm. To test the robustness of the method, we take two different initializations shown in Figure 5a and in Figure 5c. Both reconstructions (Figure 5b and Figure 5d) turn to be good approximations of the target shape.

6. CONCLUSION AND FUTURE WORKS

In this paper, we introduced an inverse problem, based on a direct eddy current model, to characterize the shape of magnetic deposits outside the SG tubes by using ECT signals. The inverse algorithm by gradient descent shape optimization makes use of the shape derivative and is regularized, because of its ill-posedness, by introducing a boundary Laplace-Beltrami operator. Compared to the contrast source inverse method in preceding works, the shape optimization method gives a shape estimate with precise continuous edge. Reconstruction results with *a priori* information (parameterized shape for exemple) are quite satisfying. General reconstruction gives a good volume valuation.

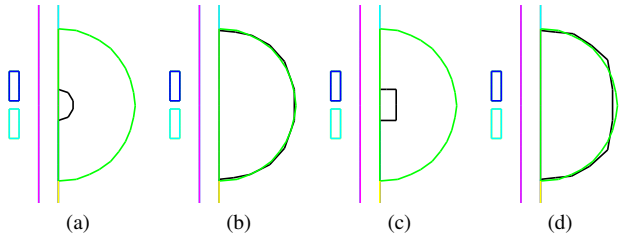

Figure 5: General problem with semi-disc shaped deposit target. In green: target shape. In black: (a)-(b) initialization with small semi-disc and reconstruction; (c)-(d) initialization with small rectangular and reconstruction.

Extensions, which may bring both mathematical and numerical difficulties, will be considered in our future works: more complicated geometrical configuration, physical nature of deposit as unknown factor to be reconstructed in the inverse problem, generalization to the 3-D case, etc.

REFERENCES

[1] G. Allaire, *Conception optimale de structures*, Springer, 2007.

[2] B. A. Auld, J. C. Moulder, "Review of Advances in Quantitative Eddy Current Nondestructive Evaluation", *Journal of Nondestructive Evaluation*, Vol. 18, No.1, 1999.

[3] H. W. Engl, M. Hanke, A. Neubauer, *Regularization of Inverse Problems*, Kluwer Academic Publishers, 1996.

[4] G. Pichenot, D. Premel, T. Sollier, V. Maillot, "Development of a 3D Electromagnetic Model for Eddy Current Tubing Inspection: Application to Steam Generator Tubing", *AIP Conference Proceedings*, Vol. 700, pp. 321-328, 2004.

[5] A. Trillon, A. Girard, J. Idier, Y. Goussard, F. Sirois, S. Dubost, N. Paul, "Eddy Current Tomography Based on a Finite Difference Forward Model with Additive Regularization", *AIP Conference Proceedings*, Vol. 1211, pp. 782-789, 2010.